

Exosomes surf on filopodia to enter cells at endocytic hot spots, traffic within endosomes, and are targeted to the ER

Wolf Heusermann,¹ Justin Hean,^{1,2} Dominic Trojer,¹ Emmanuelle Steib,¹ Stefan von Bueren,¹ Alexandra Graff-Meyer,³ Christel Genoud,³ Katrin Martin,⁴ Nicolas Pizzato,¹ Johannes Voshol,¹ David V. Morrissey,⁵ Samir E.L. Andaloussi,^{2,6} Matthew J. Wood,² and Nicole C. Meisner-Kober¹

¹Novartis Institutes for Biomedical Research, CH-4000 Basel, Switzerland

²Department of Physiology, Anatomy, and Genetics, University of Oxford, Oxford OX1 3QX, England, UK

³Friedrich-Miescher Institute for Biomedical Research, CH-4000 Basel, Switzerland

⁴Department of Biomedicine, University of Basel, CH-4058 Basel, Switzerland

⁵Novartis Institutes for Biomedical Research, Cambridge, MA 02139

⁶Department of Laboratory Medicine, Karolinska Institutet, SE-141 86 Huddinge, Sweden

Exosomes are nanovesicles released by virtually all cells, which act as intercellular messengers by transfer of protein, lipid, and RNA cargo. Their quantitative efficiency, routes of cell uptake, and subcellular fate within recipient cells remain elusive. We quantitatively characterize exosome cell uptake, which saturates with dose and time and reaches near 100% transduction efficiency at picomolar concentrations. Highly reminiscent of pathogenic bacteria and viruses, exosomes are recruited as single vesicles to the cell body by surfing on filopodia as well as filopodia grabbing and pulling motions to reach endocytic hot spots at the filopodial base. After internalization, exosomes shuttle within endocytic vesicles to scan the endoplasmic reticulum before being sorted into the lysosome as their final intracellular destination. Our data quantify and explain the efficiency of exosome internalization by recipient cells, establish a new parallel between exosome and virus host cell interaction, and suggest unanticipated routes of subcellular cargo delivery.

Introduction

Exosomes are extracellular vesicles that mediate cell-to-cell communication (Colombo et al., 2014), sometimes at a distance (Hood et al., 2011) and even between organisms (Tsu et al., 2013; Corrigan et al., 2014). They modulate recipient cell gene expression and physiology by induction of cell signaling as well as intercellular transfer of protein, lipid, and RNA cargo (Ratajczak et al., 2006; Valadi et al., 2007). They also have clinical significance because of their potential use as biomarkers (Properzi et al., 2013) or next generation therapeutics (Alvarez-Erviti et al., 2011; Kordelas et al., 2014). Hence there is need for a better understanding of how these vesicles target and enter recipient cells. The current model postulates exosome uptake via energy-dependent, receptor-mediated endocytosis (Svensson et al., 2013; Tian et al., 2013) or macropi-

nocytosis (Fitzner et al., 2011; Tian et al., 2014). Opposing models propose direct fusion with the plasma membrane (del Conde et al., 2005; Parolini et al., 2009) or phagocytosis (Feng et al., 2010). Thus, different entry routes might reflect cell specialization or conditions, and multiple entry routes might even coexist in the same cell. Further, the subcellular fate of exosomes within recipient cells and in particular their mechanisms of cargo release remains largely enigmatic. Here we report by single-vesicle dye tracing in live cells that exosomes enter cells as intact vesicles primarily via filopodia to sort into endocytic vesicle circuits that are targeted to scan the ER before being directed to the lysosome.

Results and discussion

Exosomes are efficiently taken up as single vesicles

Exosomes were labeled by transient transfection of HEK293 cells with CD63–emerald GFP (emGFP) and/or CD63–mCherry,

Correspondence to Wolf Heusermann: wolf.heusermann@unibas.ch; or Nicole C. Meisner-Kober: nicole.meisner-kober@novartis.com

W. Heusermann's present address is Imaging Core Facility, Biozentrum, University of Basel, CH-4056 Basel, Switzerland.

D.V. Morrissey's present address is Intellia Therapeutics, Inc., Cambridge, MA 02139.

Abbreviations used in this paper: CDS, coding sequence; CLSM, confocal laser scanning microscopy; DIC, differential interference contrast; emGFP, emerald GFP; FCS, fluorescence correlation spectroscopy; LNP, lipid nanoparticle; MVB, multivesicular body; NRhPE, N-rhodamine-labeled phosphatidylethanolamine; NTA, nanoparticle tracking analysis; RFP, red fluorescent protein; SPT, single particle tracking; TEM, transmission EM; TIRF, total internal reflection fluorescence.

© 2016 Heusermann et al. This article is distributed under the terms of an Attribution–Noncommercial–Share Alike–No Mirror Sites license for the first six months after the publication date (see <http://www.rupress.org/terms>). After six months it is available under a Creative Commons License (Attribution–Noncommercial–Share Alike 3.0 Unported license, as described at <http://creativecommons.org/licenses/by-nc-sa/3.0/>).

Supplemental material can be found at:
<http://doi.org/10.1083/jcb.201506084>



isolated by successive ultrafiltration and gel filtration, and concentrations were determined by fluorescence correlation spectroscopy (FCS) to enable quantification at the single vesicle level (Nordin et al., 2015). To quantify exosome cell uptake over a statistically significant number of cells, we set up a high content screening assay on a plate scanning microscope with automated image analysis. To avoid any major cell line bias, we selected cells based on a systematic profiling of parent–recipient cell pairing preferences (unpublished data) and focused on uptake of HEK293 exosomes primarily in human primary fibroblasts as well as Huh7- and HEK293-recipient cells for selected experiments. Exosome uptake levels were similar for different cell densities but declined above ~60% confluency (Fig. S1 a). Uptake was time and dose dependent, with up to 95% of Huh7 cells being targeted at 30 pM exosomes within >6 h (Fig. 1, a and c; and Fig. S1 b). The saturating characteristics indicate that a steady state between uptake and turnover is being reached and/or that the number of new vesicles entering the cell declines over time. Similar data were obtained for human primary fibroblasts (Fig. 1 b, illustrated in Fig. 1 d). We next studied exosome uptake dynamics at the single-cell level using confocal live cell imaging. Because exosomes have similar size and lipid composition as liposomal delivery vehicles, we compared the uptake dynamics of CD63-emGFP exosomes with a representative cationic lipid nanoparticle (LNP) formulation with encapsulated Cy3-siRNA. Similar vesicle concentrations were independently applied to Huh7 cells, and time-lapse confocal microscopy movies were recorded at different confocal planes. Liposomes accumulated into islands at the cell surface, which became larger over time, with only a minor fraction being endocytosed after a few hours (Fig. S1 c and Videos 1 and 2). In contrast, exosomes appeared to enter cells as single vesicles within minutes of addition without accumulation at the cell surface (Figs. 1 f and S1 d). 3D high-resolution live cell imaging with cell membrane staining confirmed that a large fraction of exosomes were indeed within the cell interior (~80% at 2 h and ~90% at 8 h) with a small fraction (~20% or 10% at 2 and 8 h, respectively) in process of binding to or crossing the plasma membrane (Fig. 1, f and g). Monitoring uptake dynamics of CD63-emGFP/CD63-mCherry double-labeled ultrafiltration and gel filtration isolated vesicles (Fig. 1 e) using single particle tracking (SPT) further corroborated that exosomes entered cells as single vesicles in virtually all recorded cell entry events (Fig. 1 h). SPT of 1,600 internalized exosomes showed that the observation time of double-labeled vesicles was statistically not shorter than that for single-labeled vesicles (Fig. S1 e), demonstrating that no separation of the two labels occurred, at least within the time that we were able to trace single particles (maximum of 20 min) and detected with the speed resolution of our system. These data would be consistent with exosomes remaining intact during and after cell entry, or their components remaining associated with the same intracellular microdomains.

Exosome uptake is clustered into filopodia active regions

Cumulative SPT visualization of exosome trajectories showed that their residency was not randomly distributed across the cell but clustered into hotspot areas near the tips of cortical actin bundles (Fig. 2 a, left) and coincided with filopodia and lamellipodia active regions (Fig. 2 a, right; Videos 3 and 4; and Fig. S1, f–j). This was not a consequence of intracellular segregation because cell entry events also clustered into the same

regions (Fig. 2 a). To uncouple the localization of filopodia from the lamellipodium, we used a line substrate, resulting in highly polarized cells persistently migrating in one direction (Martin et al., 2014) with a defined lamellipodium at the front end, filopodia distributed across the lateral regions, and retraction fibers at the back end (Fig. 2 b). Using total internal reflection fluorescence (TIRF) microscopy to focus at the bottom 200 nm where these structures are typically localized revealed that exosome cell entry trajectories were uncoupled in space and time from the lamellipodium but largely redistributed, together with filopodia, to the lateral regions (Fig. 2, c and d). This pointed to a possible direct involvement of filopodia in exosome uptake.

Exosome recruitment and cell entry is facilitated by filopodia surfing, grabbing, and pulling

Filopodia are cellular protrusions formed by actin filaments that constantly scan the environment (Mattila and Lappalainen, 2008; Bornschlöggl, 2013). Their highly dynamic movement increases the effective surface area of a cell and facilitates interaction with extracellular ligands. Moreover, the filopodial base is an area of active actin remodeling and thus a hotspot for endocytosis (Lehmann et al., 2005; Mattila and Lappalainen, 2008). The possibility of exosomes entering cells via filopodia is thus plausible. In fact, previous studies revealed that filopodia facilitate efficient cell entry of certain pathogens, including enveloped viruses (Lehmann et al., 2005; Zamudio-Meza et al., 2009). Indeed, we observed a prominent occurrence of direct contact of exosomes with filopodia (Fig. 3 a). Combining confocal fluorescence with differential interference contrast (DIC) live cell imaging allowed to monitor dynamics of exosomes simultaneously with filopodia, which are light diffracting, fine structures. This revealed different types of filopodia-facilitated exosome recruitment. Exosomes moved along filopodia and retraction fibers toward the cell body (Fig. 3 b and Videos 5 and 6), in striking analogy to a process previously introduced as filopodia surfing preceding viral uptake (Lehmann et al., 2005). Individual exosomes surfed on filopodia with relatively constant speed in the range of 0.1–0.3 $\mu\text{m/s}$. This is almost identical to velocities reported for other filopodia-surfing ligands, such as EGF-coated beads (Lidke et al., 2005) or murine leukemia virus particles (Lehmann et al., 2005), and suggests a movement with F-actin retrograde flow (Forscher and Smith, 1988; Mitchison and Kirschner, 1988; Sheetz et al., 1989; Bornschlöggl, 2013). Although we also observed examples of exosomes moving back and forth along tunneling nanotubes connecting two cells (Fig. S2, a and b), in at least 90% of >100 filopodia-surfing trajectories the exosomes moved toward the cell body immediately after contact (Fig. S2 d). In rare cases we documented an initial short movement in the opposite direction, followed by a transient stalling and redirection toward the cell body (Fig. S2 c), another parallel to viral particles (Lehmann et al., 2005). Once redirected toward the cell, exosomes again moved with relatively constant speed matching that of F-actin retrograde flow. Together these characteristics indicate that after exosome attachment, additional molecular interactions or receptor recruitment might be required to trigger an eventual coupling into F-actin retrograde flow, rather than directly hitchhiking onto a running conveyor belt. By analogy, systematic retrograde transport of EGF receptors in filopodia was shown to be triggered upon activation of the receptor tyrosine kinase (Lidke et al., 2005). Extensive studies of filopodia surfing with

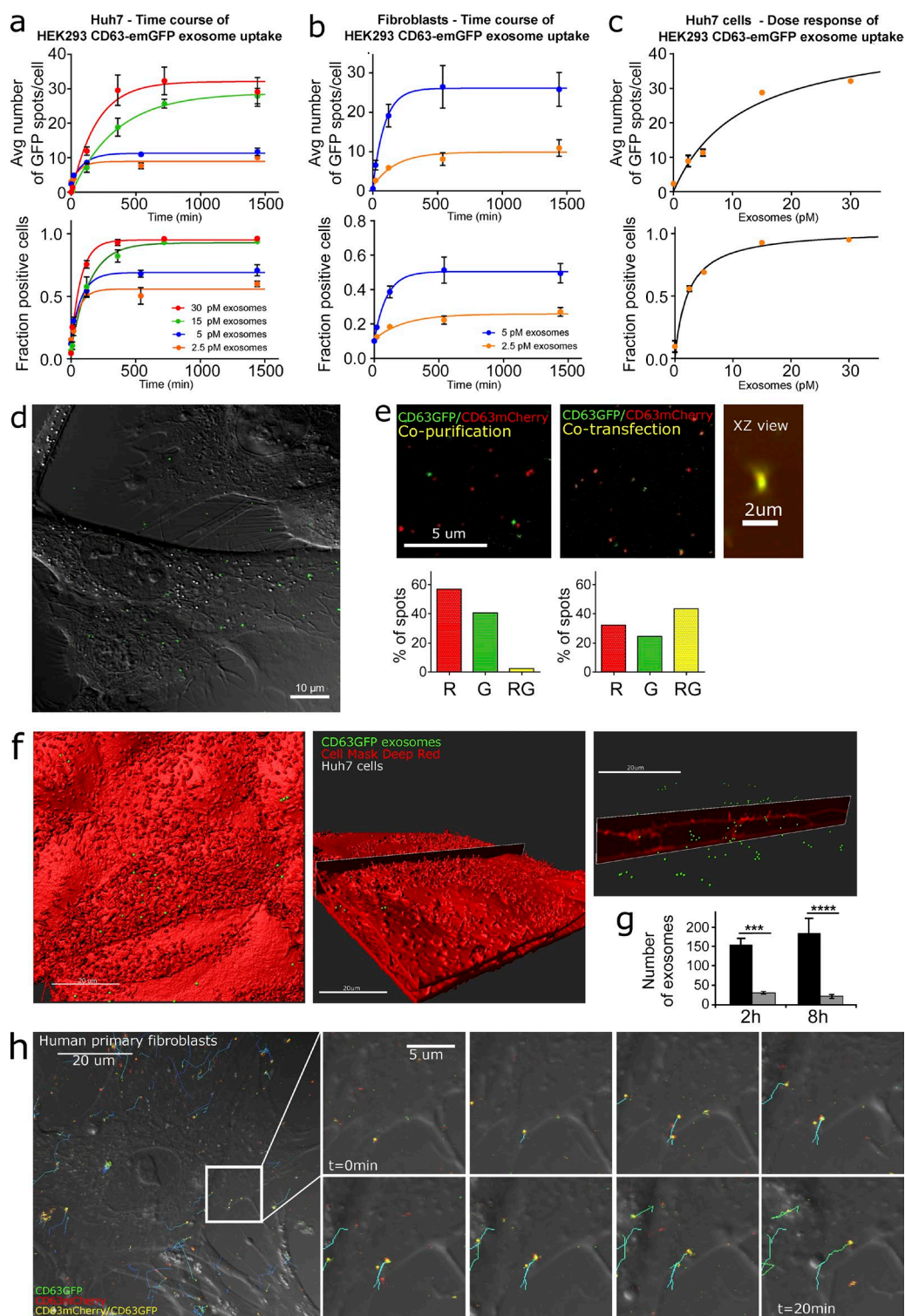


Figure 1. Quantitative exosome cell uptake dynamics. (a–c) HEK293 CD63-emGFP exosome uptake quantification using quantitative high content screening. Error bars: SD of three independent biological replicates. avg, average. (d) Human primary fibroblasts after incubation with 100 pM HEK293 CD63-GFP exosomes (green) for 10 min imaged by confocal fluorescence microscopy with DIC imaging. (e) CD63-emGFP HEK293 exosomes were copurified with CD63-mCherry exosomes and imaged by CLSM after spotting onto coverslips. The number of emGFP (G), mCherry (R), and GFP/mCherry (RG) double-positive vesicles was derived based on colocalization quantification. Vesicles were detected as light diffraction-limited emGFP or mCherry fluorescent spots of uniform size corresponding to the point spread function of the microscope with a negligible fraction of emGFP/mCherry double-positive spots, confirming recovery of single vesicles (left). Exosomes from CD63-emGFP and CD63-mCherry double-transfected cells yielded ~40% of double-labeled vesicles (middle and right). Data representative of three independent experiments. (f) High-resolution 3D images of Huh7 cells incubated with 50 pM CD63-emGFP exosomes for 2 h recorded by live cell confocal microscopy (red: CellMask DeepRed). (g) Quantification of exosomes localizing to the cell membrane versus the cell interior (Error bars: SD of three independent biological replicates, five cells per field of view; p-values, analysis of variance: ***, $P < 0.001$; ****, $P < 0.0001$). (h) SPT of CD63-emGFP/CD63-mCherry HEK293 exosome uptake in primary human fibroblasts (confocal live cell imaging, 50 s/z-stack). Trajectory statistics in Fig. S1 e.

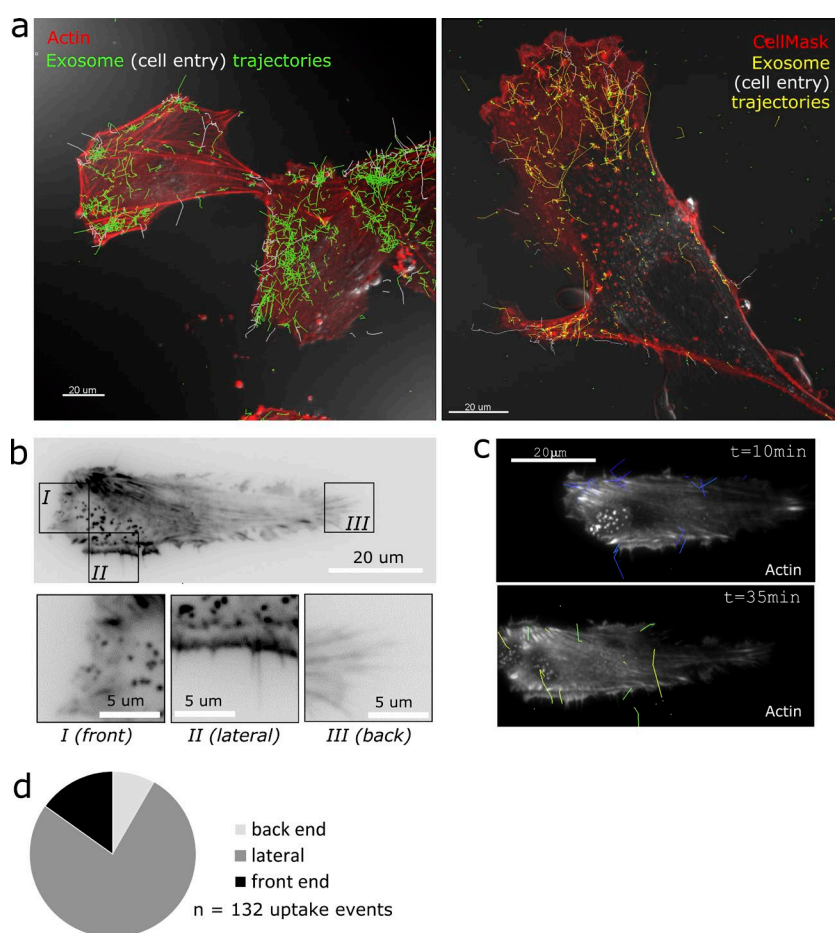


Figure 2. Exosome uptake is clustered into filopodia active regions. (a) SPT of exosome uptake dynamics by CLSM live cell imaging of actin (left) or plasma membrane-labeled (right) human primary fibroblasts. Exosomes at 100 pM; 50 s/frame. (b) TIRF live cell microscopy of stable actin-RFP expressing human fibroblasts (black) grown on line substrates. (c) Spatial distribution of cell entry events in the migrating cell with trajectories pseudocolored for absolute time within the movie. (d) Classification of exosome uptake at the front end, back end, or in the lateral region of fibroblasts on line substrates visualized by TIRF imaging (pooled data from seven independent experiments).

artificial beads have identified receptors of the integrin and cell adhesion molecule protein receptor families to couple with the filopodial actin filament. Intriguingly, both receptors had previously been implicated in exosome uptake (Morelli et al., 2004; Rana and Zöller, 2011).

In addition to surfing, two further modes of filopodia-mediated exosome recruitment were observed: contractile filopodia bound exosomes at their tips and pulled them actively to the cell surface (Fig. 3 c and Video 7), and laterally moving filopodia fished exosomes from the medium and actively hinged them to the cell body (Fig. 3 d and Video 8). To quantify the overall contribution to exosome internalization, 399 individual exosome cell entry trajectories were classified based on filopodia and nonfilopodia-mediated uptake. Strikingly, >98% of all exosome entry events occurred at the base of filopodia and retraction fibers (Figs. 4 a and S2 e). In approximately one-third of these cases we indeed documented filopodia-mediated recruitment before cell entry (Fig. 4 b), likely underestimated because of the technical limitation of visualizing these small, highly dynamic structures over a sufficiently long time frame. The predominant mode of documented exosome filopodia interaction was surfing (~25% of cell entry trajectories). Filopodia pulling and grabbing were only documented in ~3% and 1% of all cases, respectively. However, because of the rapid dynamics in 3D space of laterally moving and contractile filopodia, numbers of pulling and grabbing events might be underrepresented.

Filopodia-mediated uptake implies that actin polymerization is required already for exosome recruitment and upstream of endocytosis. Consistently, Cytochalasin D treatment of recipient

cells resulted in no major loss of exosome cell binding but an inhibition of directed and rapid movement as well as uptake (Fig. S2 f). To manipulate filopodia architecture more directly we used a small molecule (SMIFH2) which perturbs Formin-dependent actin polymerization at the barbed end, but not Arp2/3-dependent actin cytoskeleton (Rizvi et al., 2009). In line with previous studies (Barry et al., 2015; Isogai et al., 2015), short treatment with SMIFH2 (60 min) resulted in branching and eventual loss of filopodia with little to no recovery over several hours (Fig. 4 c). SMIFH2-pretreated fibroblasts showed dramatically reduced exosome uptake (Fig. 4, d and e) similar to the inhibitory effect of Heparin [in line with Christianson et al. (2013)], supporting that exosome uptake requires intact filopodia architecture and function.

Exosomes shuttle with endosomes to undergo a stop-and-go movement along the ER and are sorted to the lysosome

At the base of filopodia, exosomes were encapsulated into larger, CellMask Deep Red-labeled endocytic vesicles and were shuttled onward after cell entry (Fig. 4, f–h; Fig. S2 g; and Video 9). Consistent with live cell imaging, transmission EM (TEM) of exosomes tagged with Apex2 fused to the N terminus of CD63 with DAB detection showed internalized exosomes predominantly as intact, ~80–100-nm-sized vesicles within larger vesicles (Fig. 4 i). This does not completely rule out that exosomes might eventually use mechanisms for endosomal escape, however would imply a massive dilution of exosomal cargo into the cytoplasmic volume. In fact even for liposomal vehicles (Sahay et

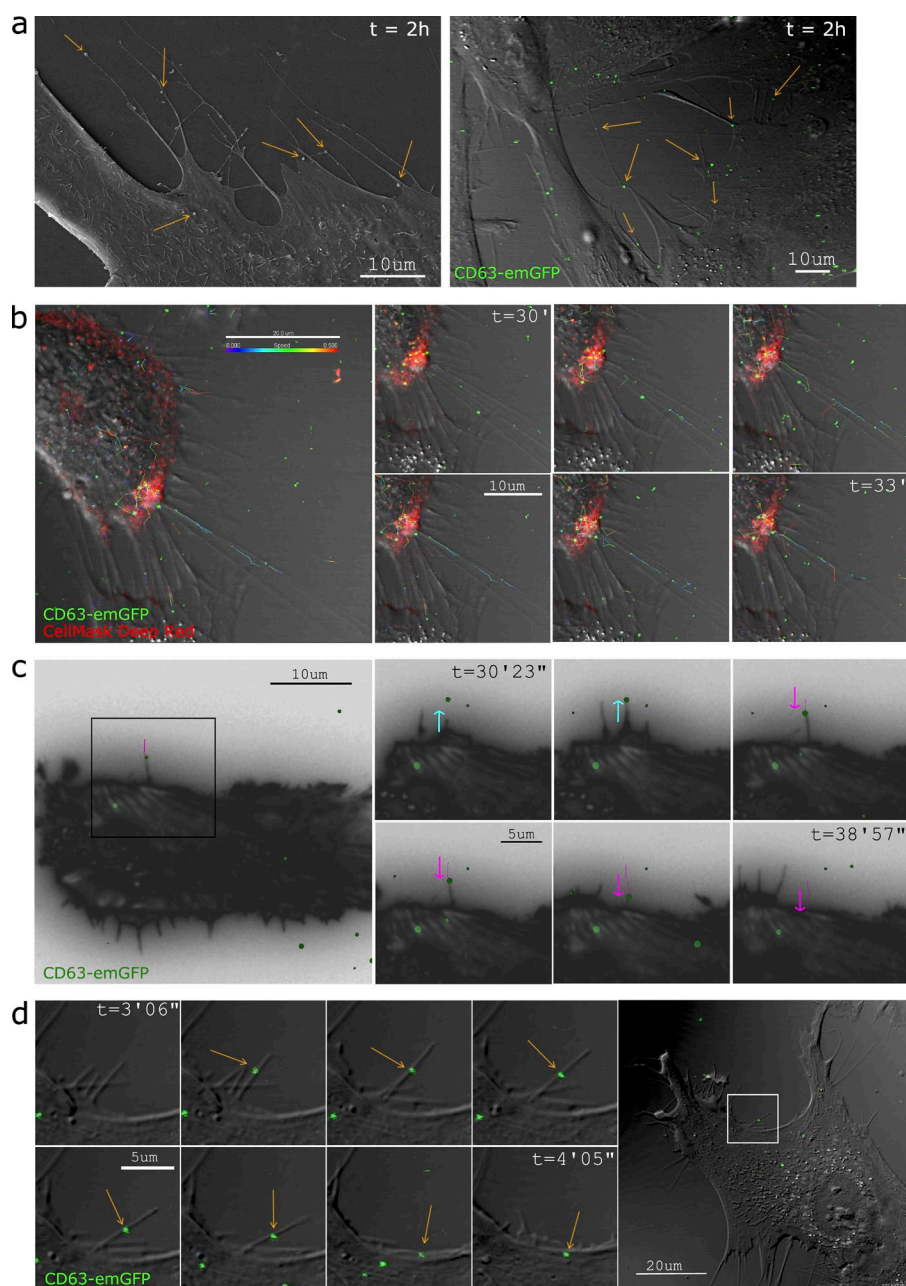


Figure 3. Exosome cell entry is facilitated by filopodia surfing, grabbing, and pulling. (a) Human primary fibroblasts incubated with 100 pM HEK293 CD63-emGFP exosomes (green). SEM (left) or live cell DIC/CLSM (right) visualization of apparent contacts of nanovesicles/exosomes with filopodia (arrows). (b) Exosome surfing on filopodia documented by live cell DIC/CLSM (Video 5, 12 frames/min). Vesicle trajectories are color coded for speed as indicated (0–0.5 $\mu m/s$). (c) Exosome pulling by filopodia documented by TIRF live cell microscopy of actin-RFP (black) expressing human fibroblasts grown on a line substrate (2 frames/min). Successive filopodia outreach and pulling movements are indicated by blue and pink arrows, respectively. Exosome trajectory in pink. (d) Grabbing of exosomes (arrows) by filopodia documented by live cell DIC/CLSM. (right) Overview image, with white box indicating the area shown in the close-up time series.

al., 2013), the concept of endosomal escape as a productive route for siRNA delivery has been challenged (Gilleron et al., 2013). It is likewise not excluded that also for exosomes, the bulk uptake does not reflect the productive population of vesicles. However, a recent study quantified that on average at least 100 exosomes need to be sampled to cover one copy of a given miRNA (Chevillet et al., 2014). Even if RNA silencing requires only a small number of RNA-induced silencing complex (RISC)-loaded siRNA or miRNA molecules per cell (Stalder et al., 2013), the above numbers imply that all or most of the cargo molecules would have to be delivered in a functional manner to reach effective concentrations. Thus the bulk uptake likely reflects a functional population. We therefore hypothesized that exosomes might sort into specific circuits to effectively reach their sites of action and set out to characterize intracellular trafficking by SPT of 312 internalized exosomes. A speed analysis (Fig. S3, a and c) revealed a stop-and-go movement for the large majority of exosomes, with peak

velocities reaching up to $\sim 8 \mu m/s$ and pronounced pauses. This was confirmed by spinning disk microscopy to rule out a bias caused by the limited time resolution by confocal laser scanning microscopy (CLSM; Fig. S3, d and e). Intracellular exosome trajectories largely followed filamentous and mesh-like structures, which were identified as ER based on labeling with ER-Tracker (Fig. 5, a and b). The stalling of exosomes typically occurred in close proximity to or at the ER, whereas the vesicles showed fast movement between different ER regions (Fig. 5 d and Videos 8 and 10). A guided movement by the ER mesh is further in line with the lack of highly straight paths apparent in the trajectory statistics (Fig. S3 b). For $\sim 90\%$ of the observed vesicles, we detected at least one close association with the ER (Fig. 5 c), with the most frequent interaction modes illustrated in Fig. 5 e and quantified in Fig. 5 f. In at least 92 out of 148 analyzed contact events, exosomes were detected within larger vesicles by DIC (Fig. 4 a). Exosome-containing endosomes showed close

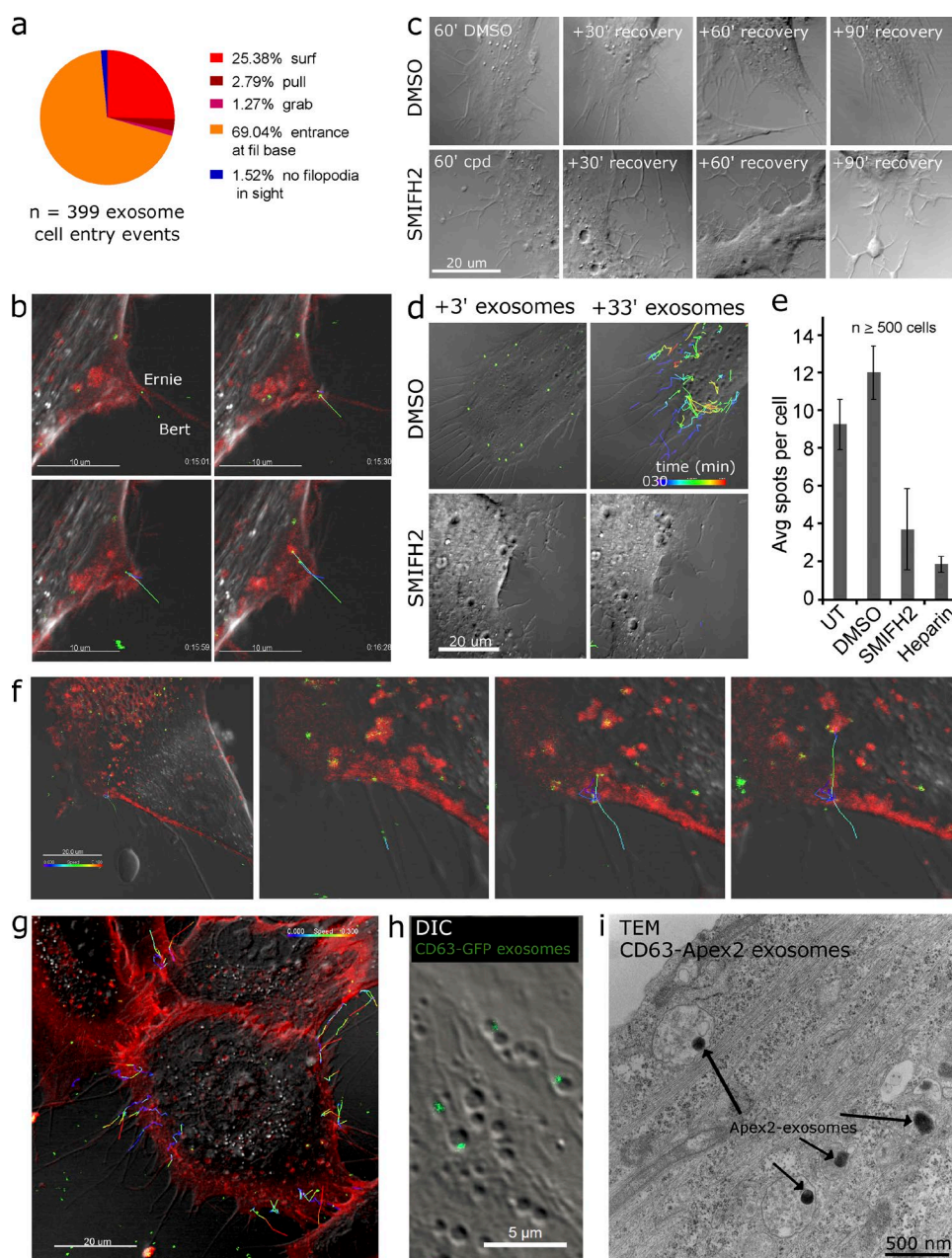


Figure 4. Exosomes are taken up at the filopodia base and shuttle with endosomes. (a) 399 individual exosome cell entry events in human primary fibroblasts documented by DIC/CLSM or TIRF microscopy were classified as indicated (pooled data from 13 independent experiments, including Videos 4, 5, and 6). (b) Ernie and Bert illustrate typical examples for exosomes classified as either filopodia surfing or entering at the filopodia base, respectively. (c) Filopodia perturbation of human primary fibroblasts pretreated for 60 min with 40 μ M SMIFH2 or DMSO at 0.5%, monitored by DIC imaging over 90 min of recovery, and (d) cumulative representation of exosome uptake trajectories in SMIFH2 versus DMSO pretreated fibroblasts by CLSM/DIC live cell imaging (exosomes at 30 pM). (e) Quantification of exosome uptake in SMIFH2 or DMSO pretreated fibroblasts by automated high content screening (exosomes at 30 pM, 2 h), as compared with exosome uptake inhibition by addition of Heparin (0.4%). Error bars: SD from three biological replicates; p-values: analysis of variance. avg, average; ***, $P < 0.001$; ****, $P < 0.0001$; ns, not significant. Representative examples of exosomes entering together with CellMask DeepRed into plasma membrane-derived endocytic vesicles (f and g) which can be visualized by DIC (h). All images represent single frames from DIC/CLSM live cell movies. Red, plasma membrane labeling (CellMask Deep Red); green, CD63-emGFP HEK293 exosomes. Exosome trajectories color coded for speed. (i) TEM visualization of CD63-Apex2-tagged exosomes (30 pM) internalized into human primary fibroblasts (4 h) using DAB staining.

association with ER filaments, tips, branches, and cavities (Fig. 5 f), highly reminiscent of the recently revealed interaction between Rab5- and Rab7-positive endosomal vesicles and the ER (Friedman et al., 2013). Thus we assessed an eventual sorting of exosomes to compartments of the late endosome by quantifying the colocalization of exosomes with Lysosomes (LysoTracker green) and multivesicular bodies (MVBs; N-rhodamine-labeled

phosphatidylethanolamine [NRhPE]) based on Bolte and Cordelières (2006) (Fig. S3, f and g). Consistent with a lack of detection of MVB localization of Apex2-tagged exosomes by TEM, Pearson coefficients demonstrated only minimal colocalization of internalized exosomes with NRhPE. However, exosomes did increasingly colocalize with lysosomes over time and reaching up to ~50–60% after 48 h in fibroblasts.

Our data demonstrate that exosomes (a) enter cells as individual vesicles within minutes upon addition, (b) show no accumulation at the cell surface but rather a seemingly “barrierless” cell penetration with (c) most detectable cell contact events leading to internalization, resulting in (d) >95% of cells being targeted within only a few hours and (e) reaching saturation at low picomolar concentrations. We therefore conclude that exosome cell uptake is highly efficient. Because these characteristics are reminiscent of effective pathogen infection rather than synthetic delivery vehicles, we propose to use the term “transduction” rather than “transfection” for exosome recipient cell targeting. We describe a new physiologic function of filopodia as highways for cell entry of exosomes, likely only hijacked by viruses and other pathogens. Of note, some filopodia-surfing viruses can promote an increased filopodia formation in their host cells through Phosphoinositide-3-kinase activation, thereby reinforcing viral invasion (Smith et al., 2008; Nobile et al., 2010). It is thus conceivable that exosomes might use similar mechanisms for feedback control of their own uptake, as exemplified by the ability of exosomes to increase tunneling nanotubes (Thayanithy et al., 2014).

At the base of filopodia, exosomes sort into endosomal trafficking circuits that are targeted to scan the ER as a possible site of cargo release (Fig. S3 h). We and others have recently revealed that siRNA as well as miRNA loading into RNA-induced silencing complex, RISC binding to target mRNA, and mRNA slicing/silencing are nucleated at the rough ER membrane (Li et al., 2013; Stalder et al., 2013). Consistently, the ER is now recognized as a nucleation site for translation in general, rather than only for secreted proteins as had long been assumed (Jagannathan et al., 2014; Reid et al., 2014; Reid and Nicchitta, 2015). A directed transport of exosomes to the ER membrane would therefore allow for an efficient entry of exosomal miRNA and mRNA cargo into the RNAi and translation machineries. Live cell movies showed a transiently coordinated movement of exosomes and ER (Videos 8 and 10), with contact events ranging from a few seconds up to 20 min (Fig. 5 e). This suggests a true interaction of ER and exosome containing vesicles rather than random crossing of their paths. In line with the live cell data, TEM imaging showed internalized CD63-Apex2 tagged exosomes predominantly as vesicles within larger vesicles in proximity to the rough ER and/or cytoskeleton (Fig. 5 g). Whether and how exosomal cargo may be released, or functionally displayed at the ER across the endosomal (and exosomal) double-lipid membranes, as well as what factors may license vesicles for this specific cell entry route will be important questions for future studies. By adding another layer to the previously noted convergence with viral pathways (Wurdinger et al., 2012), we anticipate that our data open up new links for translating viral mechanisms to advance exosome biology.

Materials and methods

Parent cells

Human embryonic kidney cells (HEK293; ATCC) were cultured in complete media comprised of DMEM (Life Technologies), supplemented with 10% FBS (Cellgro) and penicillin/streptomycin (5 mg/ml; Cellgro) at 37°C with 5% CO₂. For fluorescent exosome labeling, the full-length coding sequence of human CD63 isoform A (available from GenBank under accession no. NM_001257390.1) was TOPO cloned into the pcDNA 6.2 N-emGFP vector (Promega) to result in an N-terminal fusion of emGFP to CD63. pcDNA 6.2 N-mCherry-CD63

and N-mCherry-emGFP-CD63 vectors were then subcloned by replacing the emGFP coding sequence (CDS) in between the Ava I sites by gene synthesized inserts (Solvias) comprising the CDS of either mCherry or an emGFP-mCherry fusion. For tagging of exosomes for TEM, the Apex2 CDS (Lam et al., 2015) was additionally cloned in frame upstream of emGFP with additional insertion of a Flag peptide at the N terminus to result in an N-FLAG-Apex2-emGFP-CD63 expression construct. For exosome isolation, 5–8 × 10⁶ HEK293 cells were seeded in a 15-cm culture dish with complete media and transfected with CD63 expression constructs the next day. Cell transfection was done in complete medium using Lipofectamine2000 (Life Technologies; 1 mg DNA/2.2 ml LF2000) following the manufacturer's instructions. After 4 h, cells were washed, and medium was replaced by OptiMEM. Conditioned media were collected after 48 h for exosome isolation. Typically, 100–200 ml of conditioned medium (pooled from multiple dishes) was used in most experiments.

Recipient cells

Human primary fibroblasts from a healthy donor (C-013-5C; Life Technologies) were grown in MEM (Life Technologies) supplemented with 15% FBS and penicillin/streptomycin (5 µg/ml) in 0.1% gelatin (Sigma-Aldrich) coated T150 flasks. For exosome uptake experiments, cells were either plated in eight-well slides (ibidi) at a density of 40–60% (confocal and DIC live cell imaging experiments) or 96-well plates (iBiTreat; ibidi) at a density of 60% (exosome uptake high content screening assay). Transient expression of Adeno-Lifeact-mCherry in human fibroblast cells was obtained by adenoviral transduction, and cells were seeded onto line substrates or 2D substrates (Fibronectin-coated coverslips) at least 6 h before TIRF live cell imaging. Line substrate microfabrication was performed as described in detail elsewhere (Martin et al., 2014). In brief, surface glass coverslips coated with poly-L-Lysine/poly-ethylene-glycol and polydimethylsiloxane ridge stamps were used as a template to produce the line substrate (20-µm-wide ridge structures separated by 100-µm-wide gaps) by plasma etching followed by fibronectin coating.

Huh7 cells (HSRRB) and HEK293 cells were cultivated in DMEM supplemented with 10% FBS and 1× L-Glutamine 200 mM (Life Technologies) and penicillin/streptomycin and plated in 96-well plates at a cell density of 40–60% confluency 1 d before exosome addition.

Exosome isolation

Exosome isolation via UF/GF was essentially performed as described elsewhere (Nordin et al., 2015). In brief, conditioned medium was pre-cleared of cell debris and larger particles by consecutive centrifugation at 300 g for 5 min followed by 3,000 g for 10 min, as well as filtration over a 0.22-µm filter. Typically, 100–200 ml of the pre-cleared conditioned medium was then concentrated to a volume of 0.5–1 ml on an AMICON ultrafiltration device using a 100-kD molecular mass cutoff membrane (EMD Millipore). Enriched medium was then loaded onto a Superdex200 column (GE Healthcare) connected to an ÄKTA prime FPLC instrument (GE Healthcare) equipped with a UV flow cell. Gel filtration was performed at 4°C using sterile filtered 50 mM Tris buffer (flow rate 0.5 ml/min). 96 individual fractions of 200 µl each were collected. Nanoparticle tracking analysis (NTA) and FCS were performed directly in all fractions. Vesicle containing fractions were pooled and further characterized by Western blotting and mass spectrometry proteomics.

FCS

Exosome quantification and characterization via FCS were essentially performed as described elsewhere (Nordin et al., 2015). In brief, samples were measured on a Clarina II Reader (Evotec Technologies) with 488-nm argon ion laser excitation, a 40× water immersion 1.15 NA

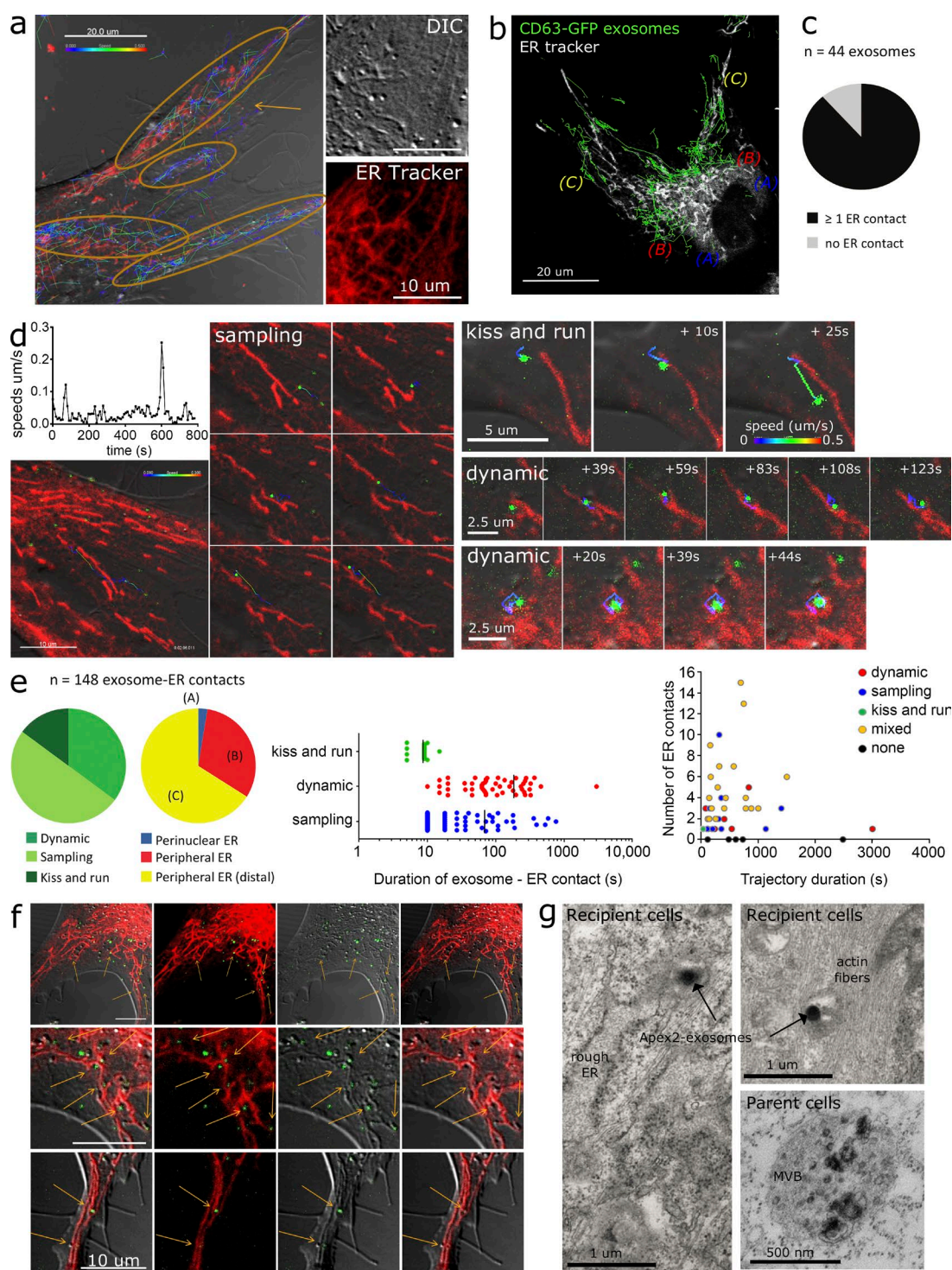


Figure 5. Internalized exosomes undergo a stop-and-go movement along the ER. (a) Cumulative intracellular exosome trajectories color coded for exosome speed (0–0.5 $\mu\text{m/s}$) in an overlay of DIC with confocal fluorescence images (left) and side by side (right). (b) Cumulative intracellular trajectories (green) show exosome residency mainly near regions of peripheral ER (B and C) but largely absent from the perinuclear region (A). (c) Fraction of intracellular exosomes for which at least one contact with the ER was detected. (d) Representative examples for predominant modes of exosome-ER interactions, with a corresponding speed trace illustrating exosome stop-and-go movement (top left). (e) Characterization of 148 individual exosome-ER contacts for interaction mode and spatial distribution (left), contact duration (middle), and number of interactions per vesicle (right). (c and e) Pooled data from three independent experiments. (d) Representative data from at least five different experiments. (f) Overlay of DIC with confocal fluorescence images (150 min after exosome addition) show exosomes localizing closely to ER filaments, tips, cavities, and branches (arrows). All images, human primary fibroblasts: green, CD63-emGFP HEK293 exosomes; red, ER Tracker. (g) TEM imaging shows CD63-Apex2-labeled exosomes upon uptake in human primary fibroblasts typically within vesicles close to rough ER and cytoskeleton. Bottom right, CD63-Apex2-transfected HEK293 parent cells.

objective (UAPO Olympus), 50- μm pinhole, and SPCM-AQR-13FC avalanche photodiode (Perkin-Elmer Optoelectronics). The confocal volume was calculated in approximation as a cylinder of radius ω_1 and height ω_2 , using the measured diffusional correlation time t_{diff} of free dye (Alexa Fluor 488; Life Technologies), the known translational diffusion coefficient of Alexa Fluor 488 (Molecular Probes; $D = 280 \mu\text{m}^2/\text{s}$), and the axis ratio AR fitted from calibration measurements to derive $\omega_1 = 4 \times D \times t_{\text{diff}}$ and $\omega_2 = \omega_1 \times AR$. The concentration of fluorescing molecules was obtained as $c = N/(N_A \times \omega_1 \times 2\pi \times \omega_2)$, where N_A is the Avogadro number and N is the number of particles in the confocal volume detected by FCS. For each sample, several dilutions were made and measured in a 96-well glass bottom plate (Whatman) with 30 repetitive measurements of 10 s each. NP-40S at 1% vol/vol (Biosciences) was used to induce vesicle disruption for determination of detergent sensitivity and quantification of CD63-emGFP molecules per exosome.

Single vesicle imaging

Exosomes from CD63-emGFP/CD63-mCherry double-transfected HEK293 cells were imaged by confocal fluorescence microscopy after spotting onto coverslips. Additionally, conditioned medium from either CD63-emGFP or CD63-mCherry transfected HEK293 cells was mixed and copurified by ultrafiltration and gel filtration, and exosomes were imaged under the same conditions. Colocalization was quantified based on overlap of the point spread functions in the two fluorescent channels to derive the number of GFP (G), mCherry (R), and GFP/mCherry (RG) double-positive vesicles.

Scanning EM

Cells were grown on Thermanox coverslips (Nunc; Thermo Fisher Scientific). After a quick wash (<10 s) in fresh culture medium without protein, cells were fixed with 2% paraformaldehyde (Electron Microscopy Science) and 2.5% glutaraldehyde (Electron Microscopy Science) in 0.1 M cacodylate buffer (Sigma-Aldrich), pH 7.4. Cells were rinsed in 0.1 M cacodylate buffer (3×5 min). Dehydration was performed in a graded ethanol series (30, 50, 70, 90, 95, and 100% ethanol, 3×2 min each step). After dehydration, specimens were rinsed with hexamethyldisilazane (Sigma-Aldrich) and dried in an oven (60°C for 2 h). Samples were mounted on aluminum stubs by fixing the coverslip with double-sided carbon tape and sputter coated (SC7620; Quorum) with gold/palladium (5–8 nm). Cells were examined with a scanning electron microscope (Versa 3D; FEI) using the ETD detector.

TEM of CD63-Apex2-tagged exosomes

Apex2 staining was done afterward (Lam et al., 2015). Cells were grown in plastic six-well plates, incubated with 30 pM Flag-Apex2-emGFP-CD63 exosomes for 4 h and then fixed for 1 h on ice with 2% glutaraldehyde and 2% paraformaldehyde in 0.1 M cacodylate buffer with 2 mM CaCl_2 , pH 7.4. Cells were rinsed and treated for 5 min in 20 mM glycine on ice before the addition of 1.4 mM DAB and 0.03% H_2O_2 in cold buffer for 5–20 min. Cells were rinsed to stop DAB reaction and postfixed with 1% osmium tetroxide (Electron Microscopy Sciences) for 30 min in cold cacodylate buffer. Cells were rinsed, stained overnight at 4°C in 1% uranyl acetate in ddH_2O , dehydrated in a graded ethanol series, and flat-embedded in Embed-812 resin (Electron Microscopy Science). After polymerization at 60°C overnight, 50-nm sections were cut and poststained with lead citrate and uranyl acetate. Sections were imaged on an 80-kV Philips CM10 transmission electron microscope equipped with a Veleta camera (EMSIS).

NTA

Label-free particle size and concentration determination was performed on an LM NTA instrument (NanoSight). With a camera gain

of 500, full detection range, and 90-s recordings, the camera settings as well as analyses parameters (detection threshold of 2, minimum expected particle size of 50 nm, and fixed minimal track length of 4) were kept constant throughout all measurements. For quantitative analysis of particle size distribution and concentration, a dilution row of samples between 1:100 and 1:10,000 was analyzed to hit the dynamic range of the instrument ($1 - 4 \times 10^8$ particles/ml).

Automated high content screening assay for exosome uptake

Cells were seeded into a 96-well plate and incubated with exosomes as indicated in each experiment. Cells were fixed for 20 min at RT with PenFix (Thermo Fisher Scientific) in presence of 1 mg/ml Hoechst (Life Technologies) and 0.02% (vol/vol) CellMask Deep Red (Life Technologies). After extensive washing with PBS, wells were imaged on an automated confocal plate scanning instrument (Operetta; Perkin Elmer) at 40 \times magnification (NA 0.95). Image analysis was done using the Harmony software (PerkinElmer), by first identifying the nuclei (Hoechst), defining the cell boundaries (CellMask Deep Red), and finally quantifying the number of GFP spots per cell. At least 5,000 cells were analyzed by condition. Data are shown from one representative experiment from at least three independent experiments and represent averages with error bars indicating SDs from three independent samples.

CLSM/DIC live cell microscopy

For combined confocal fluorescence and DIC live cell imaging, cells were seeded into an eight-well m-slide and prestained before exosome addition as indicated in each experiment; Cell membrane: CellMask Deep Red (dilution 1:1,000 for at least 2 min); MVB: NRhPE (2.5 μm , for at least 60 min; Avanti Polar Lipids); ER: ER Tracker Red (500 nM, for at least 15 min, Life Technologies); and Lysosomes: LysoTracker green (dilution 1:1,000, for at least 60 min, Life Technologies). Actin was labeled by transfection with CellLight Actin–red fluorescent protein (RFP; Life Technologies) 24 h before imaging. Images were acquired on a confocal LSM710 microscope with a Big-detector (ZEISS) and 100 \times or 63 \times oil 1.4 NA PlanApoChromat DIC objectives with temperature (37°C), gas, and humidity (5% CO_2 , >95% relative humidity) control (Life Imaging Services) in cell medium. DIC was set up using the transmission of the excitation laser as a light source and the thiopurine methyltransferase as the detector. The microscope was controlled by the Zen Black software (ZEISS), and images were visualized by Imaris software (Bitplane). To make sure we did not miss fast events or out of confocal plane events, we did additional exosome tracing with subsecond time resolution and pinhole settings to cover 8- μm optical sections per image (with parallel DIC TPMT channel at the LSM710). For colocalization studies, a Leica Sp5 (60 \times oil, NA 1.4 PlanApoChromat, including two HyD detectors) and an LSM800 (63 \times oil, NA 1.4 PlanApoChromat, including two gasp detectors) was used with multichannel/track and two-color sequential line scanning to avoid bleach-through, cross talk, and movement-dependent signal correlation. An oversampling with 130-nm z-sectioning and 40-nm xy distance was chosen for deconvolution and colocalization analysis.

TIRF live cell microscopy

For live cell TIRF imaging, human fibroblasts were transiently transfected with Adeno-Lifeact-mCherry and seeded onto line substrates or 2D substrates prepared as described in Martin et al. (2014) 4 h before acquisition. TIRF microscopy (Roper Scientific) was performed with a TI Eclipse (Nikon) inverted stand equipped with a PlanApo 60 \times TIRF Objective 1.49 NA, a Evolve EMCCD camera (Photometrics), 491- and 561-nm solid-state laser diodes and was controlled using MetaMorph imaging software (Molecular Devices). Fluorescent exosomes were quantified and characterized by FCS and typically added 5–10 min before image acquisition unless specified otherwise.

Confocal spinning disk fluorescence live cell microscopy

Rapid time-lapse imaging was performed using 3I spinning disk confocal microscope (Axio Observer, 63× 1.4 N.A and Yokogawa SD unit; ZEISS) with a stage-top incubation system creating a 37°C with 5% CO₂ environment. Z-stacks of 8–12 sections with two-channel detection were acquired every 1–3 s using an Evolve 512, backilluminated EMCCD camera (Photometrics). For live cell experiments, human primary fibroblasts or Huh7 cells were treated with 30 pM CD63-emGFP HEK293 exosomes. Cells were stained with CellMask Deep Red (dilution 1:1,000) for at least 5 min before exosome treatment. Cells were imaged for up to 5 min (30–300 z-stacks). The imaging microscope was controlled by Slidebook 6 (Intelligent Imaging), and time-lapse stacks were analyzed with Imaris 8 64x.

Filopodia manipulation with SMIFH2

Human primary fibroblasts were seeded in eight-well plates and treated with 40 μM SMIFH2 (Sigma-Aldrich) or 0.5% DMSO for 60 min. Cells were washed, and 30 pM CD63-emGFP HEK293 exosomes were added in MEM/15% FBS. Exosome dynamics was monitored by CLSM/DIC live cell imaging and analyzed by SPT as described. For quantification of exosome uptake inhibition, human primary fibroblasts were seeded in 96-well plates and treated with 40 μM SMIFH2 or DMSO at 0.5% for 60 min, and 30 pM CD63-emGFP exosomes were added in fresh medium. For Heparin treatment, exosomes were added in presence of 0.4% Heparin. After 2 h of incubation, cells were fixed with PenFix and stained with CellMask Deep Red, and uptake was quantified by the high content screening assay described above.

Image analysis

Confocal image stack time series, confocal image plane time series, and TIRF time-lapse data were imaged with frame rates and duration as indicated. Particle tracking and trajectory analysis was performed with the Imaris x64 Particle Tracking Analysis module. Unless specified otherwise, SPT trajectories are shown as dragontail visualization with a maximum of 20 frames. Speeds were derived from relative exosome displacement between two frames. For colocalization studies, z-stacks recorded with oversampling were deconvolved with Huygens remote manager (automatic threshold) and then analyzed with the JACoP plugin (Bolte and Cordelières, 2006) for Fiji. For evaluation of the ratio of internalized versus membrane bound exosomes, high-resolution confocal 3D image stacks of CellMask Deep Red membrane-labeled recipient cells (exosome incubation time as indicated) were deconvolved (Huygens) and subsequently analyzed by Imaris. The cell membrane was rendered in 3D, and exosomes were detected by spot detection. The light diffraction-limited fluorescent vesicles were represented as oversized 2-μm green spheres to visualize them at the rendered cell surface. All vesicles which were visible on top or within the membrane were counted as membrane bound, and vesicles within the membrane enclosed surface were counted as internalized vesicles.

LNP formulations

Lipid Nanoparticle siRNA formulations were provided by J. Baryza and K. Bowman (Novartis Institutes for Biomedical Research, Cambridge, MA). 5'-Cy3 labeled siRNA targeting SSB (guide: 5'-UUA CAUUAAGUCUGUUGUUU-3'; passenger: 5'-Cy3ACAACAGAC UUUAAUGUAAUU-3') was mixed in a 1:5 ratio with unlabeled siRNA and formulated as described previously in detail (Baryza et al., 2014). In brief, the LNPs were formed by mixing equal volumes of lipid solution dissolved in ethanol with siRNA dissolved in a citrate buffer by an impinging jet process. The lipid solution contained a cationic lipid (Baryza et al., 2014), a helper lipid (cholesterol), and a polyethylene glycol lipid in a ratio of 50:46:4 at a siRNA concentration

of 1 mg/ml. The LNP solution was then diafiltered with a molecular mass cutoff 100-kD membrane, sterile filtered, and stored at 4°C. The vesicles typically had a diameter of ~150 nm.

Online supplemental material

Fig. S1 shows supplemental data to quantification of CD63-emGFP uptake. Fig. S2 shows supplemental data to exosome filopodia interaction and cell entry. Fig. S3 shows supplemental data to intracellular trafficking of internalized exosomes. Video 1 shows LNP formulations accumulate at the cell surface (cell surface confocal plane). Video 2 shows LNP formulations accumulate at the cell surface (cell interior confocal plane). Video 3 shows exosome uptake in human primary fibroblasts is clustered into filopodia active regions. Video 4 shows exosomes are endocytosed in human primary fibroblasts at filopodia active regions. Video 5 shows exosome surf on filopodia of human primary fibroblasts, monitored by DIC/CLSM live cell imaging. Video 6 shows exosome surf on filopodia of human primary fibroblasts, monitored by TIRF live cell imaging. Video 7 shows fibroblast pulls exosome to cell surface. Videos 8 shows exosomes scan along the ER. Video 9 shows exosome uptake in human primary fibroblast recipient cells stained with CellMask Deep Red. Video 10 shows intracellular exosome movement. Online supplemental material is available at <http://www.jcb.org/cgi/content/full/jcb.201506084/DC1>.

Acknowledgments

We thank Jeremy Baryza and Keith Bowman for providing LNP encapsulated siRNA, Rene Hemming for guidance in setting up the gel filtration, and the Imaging Core Facility of the Biocenter/Basel for access to spinning disk, Leica SP5, and Zeiss LSM800 microscopy instruments. We further thank Nancy Hynes, Helge Grosshans, and Urs Greber for inspiring discussions.

S.E.L. Andaloussi is supported by the Vetenskapsrådet (VR-Med and EuroNanoMedII) and the Swedish Society for Medical Research.

The authors declare no competing financial interests.

Submitted: 17 June 2015

Accepted: 9 March 2016

References

- Alvarez-Erviti, L., Y. Seow, H. Yin, C. Betts, S. Lakhal, and M.J.A. Wood. 2011. Delivery of siRNA to the mouse brain by systemic injection of targeted exosomes. *Nat. Biotechnol.* 29:341–345. <http://dx.doi.org/10.1038/nbt.1807>
- Barry, D.J., C.H. Durkin, J.V. Abella, and M. Way. 2015. Open source software for quantification of cell migration, protrusions, and fluorescence intensities. *J. Cell Biol.* 209:163–180. <http://dx.doi.org/10.1083/jcb.201501081>
- Baryza, J., K. Bowman, A. Geall, T. Labonte, C. Lee, C. Vargeese, L. West, and J. Zhao. 2014. Lipids, lipid compositions, and methods of using them. U.S. Patent 2014/0309277 A1. 191, filed March 4, 2014 and issued October 16, 2014.
- Bolte, S., and F.P. Cordelières. 2006. A guided tour into subcellular colocalization analysis in light microscopy. *J. Microsc.* 224:213–232. <http://dx.doi.org/10.1111/j.1365-2818.2006.01706.x>
- Bornschlög, T. 2013. How filopodia pull: what we know about the mechanics and dynamics of filopodia. *Cytoskeleton (Hoboken)*. 70:590–603. <http://dx.doi.org/10.1002/cm.21130>
- Chevillet, J.R., Q. Kang, I.K. Ruf, H.A. Briggs, L.N. Vojtech, S.M. Hughes, H.H. Cheng, J.D. Arroyo, E.K. Meredith, E.N. Gallichotte, et al. 2014. Quantitative and stoichiometric analysis of the microRNA content of exosomes. *Proc. Natl. Acad. Sci. USA*. 111:14888–14893. <http://dx.doi.org/10.1073/pnas.1408301111>

- Christianson, H.C., K.J. Svensson, T.H. van Kuppevelt, J.-P. Li, and M. Belting. 2013. Cancer cell exosomes depend on cell-surface heparan sulfate proteoglycans for their internalization and functional activity. *Proc. Natl. Acad. Sci. USA*. 110:17380–17385. <http://dx.doi.org/10.1073/pnas.1304266110>
- Colombo, M., G. Raposo, and C. Théry. 2014. Biogenesis, secretion, and intercellular interactions of exosomes and other extracellular vesicles. *Annu. Rev. Cell Dev. Biol.* 30:255–289. <http://dx.doi.org/10.1146/annurev-cellbio-101512-122326>
- Corrigan, L., S. Redhai, A. Leiblich, S.-J. Fan, S.M.W. Perera, R. Patel, C. Gandy, S.M. Wainwright, J.F. Morris, F. Hamdy, et al. 2014. BMP-regulated exosomes from *Drosophila* male reproductive glands reprogram female behavior. *J. Cell Biol.* 206:671–688. <http://dx.doi.org/10.1083/jcb.201401072>
- del Conde, I., C.N. Shrimpton, P. Thiagarajan, and J.A. López. 2005. Tissue-factor-bearing microvesicles arise from lipid rafts and fuse with activated platelets to initiate coagulation. *Blood*. 106:1604–1611. <http://dx.doi.org/10.1182/blood-2004-03-1095>
- Feng, D., W.-L. Zhao, Y.-Y. Ye, X.-C. Bai, R.-Q. Liu, L.-F. Chang, Q. Zhou, and S.-F. Sui. 2010. Cellular internalization of exosomes occurs through phagocytosis. *Traffic*. 11:675–687. <http://dx.doi.org/10.1111/j.1600-0854.2010.01041.x>
- Fitzner, D., M. Schnaars, D. van Rossum, G. Krishnamoorthy, P. Dibaj, M. Bakhti, T. Regen, U.-K. Hanisch, and M. Simons. 2011. Selective transfer of exosomes from oligodendrocytes to microglia by macropinocytosis. *J. Cell Sci.* 124:447–458. <http://dx.doi.org/10.1242/jcs.074088>
- Forscher, P., and S.J. Smith. 1988. Actions of cytochalasins on the organization of actin filaments and microtubules in a neuronal growth cone. *J. Cell Biol.* 107:1505–1516. <http://dx.doi.org/10.1083/jcb.107.4.1505>
- Friedman, J.R., J.R. Dibenedetto, M. West, A.A. Rowland, and G.K. Voeltz. 2013. Endoplasmic reticulum-endosome contact increases as endosomes traffic and mature. *Mol. Biol. Cell*. 24:1030–1040. <http://dx.doi.org/10.1091/mbc.E12-10-0733>
- Gillerson, J., W. Querbes, A. Zeigerer, A. Borodovsky, G. Marsico, U. Schubert, K. Manygoats, S. Seifert, C. Andree, M. Stöter, et al. 2013. Image-based analysis of lipid nanoparticle-mediated siRNA delivery, intracellular trafficking and endosomal escape. *Nat. Biotechnol.* 31:638–646. <http://dx.doi.org/10.1038/nbt.2612>
- Hood, J.L., R.S. San, and S.A. Wickline. 2011. Exosomes released by melanoma cells prepare sentinel lymph nodes for tumor metastasis. *Cancer Res.* 71:3792–3801. <http://dx.doi.org/10.1158/0008-5472.CAN-10-4455>
- Isogai, T., R. van der Kammen, and M. Innocenti. 2015. SMIFH2 has effects on Formins and p53 that perturb the cell cytoskeleton. *Sci. Rep.* 5:9802. <http://dx.doi.org/10.1038/srep09802>
- Jagannathan, S., D.W. Reid, A.H. Cox, and C.V. Nicchitta. 2014. De novo translation initiation on membrane-bound ribosomes as a mechanism for localization of cytosolic protein mRNAs to the endoplasmic reticulum. *RNA*. 20:1489–1498. <http://dx.doi.org/10.1261/rna.045526.114>
- Kordelas, L., V. Rebmann, A.-K. Ludwig, S. Radtke, J. Ruesing, T.R. Doeppner, M. Epple, P.A. Horn, D.W. Beelen, and B. Giebel. 2014. MSC-derived exosomes: a novel tool to treat therapy-refractory graft-versus-host disease. *Leukemia*. 28:970–973.
- Lam, S.S., J.D. Martell, K.J. Kamer, T.J. Deerinc, M.H. Ellisman, V.K. Mootha, and A.Y. Ting. 2015. Directed evolution of APEX2 for electron microscopy and proximity labeling. *Nat. Methods*. 12:51–54. <http://dx.doi.org/10.1038/nmeth.3179>
- Lehmann, M.J., N.M. Sherer, C.B. Marks, M. Pypaert, and W. Mothes. 2005. Actin- and myosin-driven movement of viruses along filopodia precedes their entry into cells. *J. Cell Biol.* 170:317–325. <http://dx.doi.org/10.1083/jcb.200503059>
- Li, S., L. Liu, X. Zhuang, Y. Yu, X. Liu, X. Cui, L. Ji, Z. Pan, X. Cao, B. Mo, et al. 2013. MicroRNAs inhibit the translation of target mRNAs on the endoplasmic reticulum in *Arabidopsis*. *Cell*. 153:562–574. <http://dx.doi.org/10.1016/j.cell.2013.04.005>
- Lidke, D.S., K.A. Lidke, B. Rieger, T.M. Jovin, and D.J. Arndt-Jovin. 2005. Reaching out for signals: filopodia sense EGF and respond by directed retrograde transport of activated receptors. *J. Cell Biol.* 170:619–626. <http://dx.doi.org/10.1083/jcb.200503140>
- Martin, K., M. Vilela, N.L. Jeon, G. Danuser, and O. Pertz. 2014. A growth factor-induced, spatially organizing cytoskeletal module enables rapid and persistent fibroblast migration. *Dev. Cell*. 30:701–716. <http://dx.doi.org/10.1016/j.devcel.2014.07.022>
- Mattila, P.K., and P. Lappalainen. 2008. Filopodia: molecular architecture and cellular functions. *Nat. Rev. Mol. Cell Biol.* 9:446–454. <http://dx.doi.org/10.1038/nrm2406>
- Mitchison, T., and M. Kirschner. 1988. Cytoskeletal dynamics and nerve growth. *Neuron*. 1:761–772. [http://dx.doi.org/10.1016/0896-6273\(88\)90124-9](http://dx.doi.org/10.1016/0896-6273(88)90124-9)
- Morelli, A.E., A.T. Larregina, W.J. Shufesky, M.L.G. Sullivan, D.B. Stolz, G.D. Papworth, A.F. Zahorchak, A.J. Logar, Z. Wang, S.C. Watkins, et al. 2004. Endocytosis, intracellular sorting, and processing of exosomes by dendritic cells. *Blood*. 104:3257–3266. <http://dx.doi.org/10.1182/blood-2004-03-0824>
- Nobile, C., D. Rudnicka, M. Hasan, N. Aulner, F. Porrot, C. Machu, O. Renaud, M.-C. Prévost, C. Hivroz, O. Schwartz, and N. Sol-Foulon. 2010. HIV-1 Nef inhibits ruffles, induces filopodia, and modulates migration of infected lymphocytes. *J. Virol.* 84:2282–2293. <http://dx.doi.org/10.1128/JVI.02230-09>
- Nordin, J.Z., Y. Lee, P. Vader, I. Mäger, H.J. Johansson, W. Heusermann, O.P.B. Wiklander, M. Hallbrink, Y. Seow, J.J. Bultema, et al. 2015. Ultrafiltration with size-exclusion liquid chromatography for high yield isolation of extracellular vesicles preserving intact biophysical and functional properties. *Nanomedicine (Lond.)*. 11:879–883.
- Parolini, I., C. Federici, C. Raggi, L. Lugini, S. Palleschi, A. De Milito, C. Coscia, E. Iessi, M. Logozzi, A. Molinari, et al. 2009. Microenvironmental pH is a key factor for exosome traffic in tumor cells. *J. Biol. Chem.* 284:34211–34222. <http://dx.doi.org/10.1074/jbc.M109.041152>
- Properzi, F., M. Logozzi, and S. Fais. 2013. Exosomes: the future of biomarkers in medicine. *Biomarkers Med.* 7:769–778. <http://dx.doi.org/10.2217/bmm.13.63>
- Rana, S., and M. Zöller. 2011. Exosome target cell selection and the importance of exosomal tetraspanins: a hypothesis. *Biochem. Soc. Trans.* 39:559–562. <http://dx.doi.org/10.1042/BST0390559>
- Ratajczak, J., K. Miekus, M. Kucia, J. Zhang, R. Reza, P. Dvorak, and M.Z. Ratajczak. 2006. Embryonic stem cell-derived microvesicles reprogram hematopoietic progenitors: evidence for horizontal transfer of mRNA and protein delivery. *Leukemia*. 20:847–856. <http://dx.doi.org/10.1038/sj.leu.2404132>
- Reid, D.W., and C.V. Nicchitta. 2015. Diversity and selectivity in mRNA translation on the endoplasmic reticulum. *Nat. Rev. Mol. Cell Biol.* 16:221–231.
- Reid, D.W., Q. Chen, A.S.-L. Tay, S. Shenolikar, and C.V. Nicchitta. 2014. The unfolded protein response triggers selective mRNA release from the endoplasmic reticulum. *Cell*. 158:1362–1374. <http://dx.doi.org/10.1016/j.cell.2014.08.012>
- Rizvi, S.A., E.M. Neidt, J. Cui, Z. Feiger, C.T. Skau, M.L. Gardel, S.A. Kozmin, and D.R. Kovar. 2009. Identification and characterization of a small molecule inhibitor of formin-mediated actin assembly. *Chem. Biol.* 16:1158–1168. <http://dx.doi.org/10.1016/j.chembiol.2009.10.006>
- Sahay, G., W. Querbes, C. Alabi, A. Eltoukhy, S. Sarkar, C. Zurenko, E. Karagiannis, K. Love, D. Chen, R. Zoncu, et al. 2013. Efficiency of siRNA delivery by lipid nanoparticles is limited by endocytic recycling. *Nat. Biotechnol.* 31:653–658. <http://dx.doi.org/10.1038/nbt.2614>
- Sheetz, M.P., S. Turney, H. Qian, and E.L. Elson. 1989. Nanometre-level analysis demonstrates that lipid flow does not drive membrane glycoprotein movements. *Nature*. 340:284–288. <http://dx.doi.org/10.1038/340284a0>
- Smith, J.L., S.K. Campos, A. Wandinger-Ness, and M.A. Ozbun. 2008. Caveolin-1-dependent infectious entry of human papillomavirus type 31 in human keratinocytes proceeds to the endosomal pathway for pH-dependent uncoating. *J. Virol.* 82:9505–9512. <http://dx.doi.org/10.1128/JVI.01014-08>
- Stalder, L., W. Heusermann, L. Sokol, D. Trojer, J. Wirz, J. Hean, A. Fritzsche, F. Aeschmann, V. Pflanzagl, P. Basselet, et al. 2013. The rough endoplasmic reticulum is a central nucleation site of siRNA-mediated RNA silencing. *EMBO J.* 32:1115–1127. <http://dx.doi.org/10.1038/emboj.2013.52>
- Svensson, K.J., H.C. Christianson, A. Wittrup, E. Bourseau-Guilmain, E. Lindqvist, L.M. Svensson, M. Mörgelin, and M. Belting. 2013. Exosome uptake depends on ERK1/2-heat shock protein 27 signaling and lipid Raft-mediated endocytosis negatively regulated by caveolin-1. *J. Biol. Chem.* 288:17713–17724. <http://dx.doi.org/10.1074/jbc.M112.445403>
- Thayanithy, V., V. Babatunde, E.L. Dickson, P. Wong, S. Oh, X. Ke, A. Barlas, S. Fujisawa, Y. Romin, A.L. Moreira, et al. 2014. Tumor exosomes induce tunneling nanotubes in lipid raft-enriched regions of human mesothelioma cells. *Exp. Cell Res.* 323:178–188. <http://dx.doi.org/10.1016/j.yexcr.2014.01.014>
- Tian, T., Y.-L. Zhu, F.-H. Hu, Y.-Y. Wang, N.-P. Huang, and Z.-D. Xiao. 2013. Dynamics of exosome internalization and trafficking. *J. Cell. Physiol.* 128:1487–1495. <http://dx.doi.org/10.1002/jcp.24304>
- Tian, T., Y.-L. Zhu, Y.-Y. Zhou, G.-F. Liang, Y.-Y. Wang, F.-H. Hu, and Z.-D. Xiao. 2014. Exosome uptake through clathrin-mediated endocytosis and macropinocytosis and mediating miR-21 delivery. *J. Biol. Chem.* 289:22258–22267. <http://dx.doi.org/10.1074/jbc.M114.588046>
- Twu, O., N. de Miguel, G. Lustig, G.C. Stevens, A.A. Vashisht, J.A. Wohlschlegel, and P.J. Johnson. 2013. *Trichomonas vaginalis* exosomes deliver cargo

- to host cells and mediate host:parasite interactions. *PLoS Pathog.* 9:e1003482. <http://dx.doi.org/10.1371/journal.ppat.1003482>
- Valadi, H., K. Ekström, A. Bossios, M. Sjöstrand, J.J. Lee, and J.O. Lötvall. 2007. Exosome-mediated transfer of mRNAs and microRNAs is a novel mechanism of genetic exchange between cells. *Nat. Cell Biol.* 9:654–659. <http://dx.doi.org/10.1038/ncb1596>
- Wurdinger, T., N.N. Gatsen, L. Balaj, B. Kaur, X.O. Breakefield, and D.M. Pegtel. 2012. Extracellular vesicles and their convergence with viral pathways. *Adv. Virol.* 2012:767694. <http://dx.doi.org/10.1155/2012/767694>
- Zamudio-Meza, H., A. Castillo-Alvarez, C. González-Bonilla, and I. Meza. 2009. Cross-talk between Rac1 and Cdc42 GTPases regulates formation of filopodia required for dengue virus type-2 entry into HMEC-1 cells. *J. Gen. Virol.* 90:2902–2911. <http://dx.doi.org/10.1099/vir.0.014159-0>